RSC Advances

PAPER

View Article Online
View Journal | View Issue

Cite this: *RSC Adv.*, 2017, **7**, 29227

Water-based synthesis of zeolitic imidazolate framework-8 for CO_2 capture†

Zhuo Shi,[a] Yinghao Yu,*[a] Chao Fu,[b] Lefu Wang[a] and Xuehui Li[a]

Received 1st May 2017
Accepted 28th May 2017

DOI: 10.1039/c7ra04875k

rsc.li/rsc-advances

This paper studies the impacts of five key synthesis parameters of zeolitic imidazolate framework-8 (ZIF-8) in an aqueous solution, namely zinc resource, pH value, temperature, reaction time, and the concentration of water in the ligand (H_2O/Hmim). It was found that the crystallization of ZIF-8 samples is strongly impacted by these synthesis parameters. ZIF-8 synthesized at a temperature of 85 °C, reaction time of 5 min, and pH value of 11.4 had a large special surface area and pore volume, and thus had a high CO_2 adsorption capacity of 3.04 mmol g^{-1}. The CO_2 capture capacity remained constant after eleven consecutive adsorption–desorption experiments. Further applications of the hydrothermal synthesis method are promising considering the remarkable CO_2 adsorption capacity and cyclic regeneration ability.

1. Introduction

CO_2 is one of the major anthropogenic greenhouse gases, accounting for about 80% of all greenhouse gas emissions.[1] Currently, the carbon dioxide concentration in the atmosphere stands at 404 ppm, which is 120 ppm higher than that in pre-industrial times.[2] High CO_2 concentration leads to the greenhouse effect, affecting the climatic environment as well as people's lives.[3] It becomes more and more important to capture CO_2 effectively and efficiently. A commonly used method of capturing CO_2 is based on the chemical absorption using dilute aqueous solutions of alkanolamines.[4] This method is advantageous due to the simple operation and high absorption capacity. However, the energy demand of regeneration is relatively high.[5] In addition, the corrosion and degradation of the amine solution cannot be neglected.[6,7]

A large number of efforts have been devoted to developing new technologies for CO_2 capture.[8–11] Yaghi *et al.*[12] have systematically synthesized and named a series of zeolitic imidazolate frameworks (ZIFs), and successfully applied them to CO_2 capture. ZIFs are a new type of metal organic frameworks (MOFs) with high porosity, ultrahigh specific surface area, low density and adjustable channel. Meanwhile, ZIFs have structures analogous to traditional inorganic zeolites which have similar properties, such as high thermal stability and chemical stability in a variety of organic solvents, acid or alkali solution.[13] As one of the typical ZIFs, zeolitic imidazolate framework-8 (ZIF-8) is formed with transition metal cations (*e.g.* Zn^{2+}) and 2-methylimidazole anions, which has been widely used as a CO_2 adsorbent.[14–22] The traditional synthesis method of ZIF-8 is the solvent thermal synthesis in one given organic solvent in large quantities, such as methanol,[23] *N*,*N*-dimethyl formamide,[24] acetone[25] and so on. However, organic solvents are generally expensive and inevitably cause potential pollution to the environment. Moreover, organic solvents may interact with ZIF-8, and thus reside in the particle which are difficult to be removed in the subsequent separation processes.[26] Other methods have since been developed, such as mechanochemistry,[27] microwave,[28] ultrasonic method[29] and micro-emulsion synthesis.[30] However, the operation is relatively complex and often needs appropriate special techniques to assist the synthesis. A simple synthesis method is reasonably the first choice particularly for industrial applications. Pan *et al.*[31] reported the first method for rapid synthesis of ZIF-8 in an aqueous system in 2011. Not only the reaction time is considerably shortened to 5 min, but also the reaction is operated at room temperature. Although this is a great improvement for synthesizing ZIF-8, the usage of ligands during synthesis must be excessive. The minimum ratio between the ligand and the zinc resources is at least 70 since the deprotonation of 2-methylimidazole is difficult in the aqueous solution. To improve the atom economy, many studies have focused on reducing the amount of 2-methylimidazole used in the process of hydrothermal synthesis.[32–34]

It is well acknowledged that the morphology and size of the particles have great influence on the physical and chemical properties of the crystals. A large number of studies show that the synthesis parameters of ZIFs play a key role on the morphology and size.[35–41] Although those studies reported the influences of reaction parameters on the morphology and size of ZIF-8 during the process of synthesis, the effects on the CO_2 adsorption capacity are rarely considered. In this study, we not only investigate the main operating parameters in the synthesis

[a]*School of Chemistry and Chemical Engineering, South China University of Technology, Guangzhou 510640, China. E-mail: ceyhyu@scut.edu.cn; Fax: +86 20 8711 4707; Tel: +86 20 8711 4707*

[b]*SINTEF Energy Research, 7465 Trondheim, Norway*

† Electronic supplementary information (ESI) available: Tables S1–S5 and Fig. S1. See DOI: 10.1039/c7ra04875k

process, but also further present the evidence linking them with the CO_2 adsorption capacity.

2. Experimental

2.1 Materials

$Zn(NO_3)_2 \cdot 6H_2O$, $Zn(OAc)_2 \cdot 2H_2O$, $ZnSO_4 \cdot 7H_2O$, $ZnCl_2$, and 2-methylimidazole were analytical grade and purchased from Shanghai Macklin Biochemical Technology Co., Ltd (Shanghai, China). He (99.999%) and 15.0% CO_2 (in He balance, v/v) were obtained from Guangzhou Zhuozheng Gas Co., Ltd (Guangzhou, China). All the raw resources in the Experiment section were purchased and directly used without further processing.

2.2 Synthesis of ZIF-8

ZIF-8 was synthesized based on the method reported by Chen *et al.*,[32] with modified synthesis parameters. In this work, the zinc source and 2-methylimidazole were dissolved in a certain amount of water separately. These two solutions were then rapidly mixed, and kept stirring for a certain time. The mixture was then washed with water (50 mL × 3), and the particles were separated by centrifugation at 10 000 rpm for 10 min. The particles were collected after being dehydrated at 65 °C for 12 h. The details of the synthesis parameters are shown in Tables S1–S5 in the ESI.†

2.3 Characterization

The XRD peaks were obtained with a Bruker D-8 ADVANCE diffractometer (Rigaku, Japan) using a CuKα-ray source (40 kV, 40 mA) with a scanning step of 0.02° in the range of 5–50°. The relative crystallinity of the ZIF-8 samples is based on the major peak at 2θ value of 7.30° and the crystal surface (110), which is defined by the formula (1) as follows:

$$\text{Relative crystallinity} = \frac{\text{peak intensity of sample at (110) plane}}{\text{peak intensity of reference at (110) plane}} \times 100\% \quad (1)$$

N_2 adsorption–desorption experiments were performed with the micrometrics ASAP-2010 adsorption analyzer (Micromeritics, America). The samples were degassed at 150 °C in a vacuum for 6 h before the measurement to remove guest molecules. The FESEM images were taken with the PHILPS XL-30ESEM Field-Emission Scanning Electron Microscope (Carl Zeiss, Germany) at magnification 50k× with an acceleration voltage of 0.2–30 kV. The samples were coated with aurum before scanning because the ZIF-8 samples could not efficiently conduct electricity. The TGA tests were performed with the STA449 F3 thermo-gravimetric analyser (Netzsch, Germany) in the air atmosphere from 25 °C to 800 °C.

2.4 CO_2 adsorption measurement

The CO_2 adsorption measurements were carried out using breakthrough curves in packed columns on a 0.1 g scale. The adsorbent was firstly treated at 200 °C for 30 min with the He gas at the flow rate of 30 mL min^{-1}. It was then cooled to the desired adsorption temperature (35–75 °C, in an increment of 10 °C), which covers the typical temperature range of the flue gas. The flow of gas was then changed to 15.0 vol% CO_2 in the He balance at the flow rate of 30 mL min^{-1}. The adsorption was continued until saturation was achieved. The breakthrough curves were recorded. The CO_2 adsorption capacity q was calculated by the formula (2) as follows:

$$q(\text{mmol g}^{-1}) = \frac{1}{m}\int_0^t Q(C_0 - C)\mathrm{d}t \quad (2)$$

where, m is the dry weight of the adsorbents (g), Q is the influent flow rate (mL s^{-1}), C_0 and C are the inlet and outlet carbon dioxide concentration (vol%).

The stability of the ZIF-8 samples during the prolonged cyclic CO_2 adsorption was investigated for 11 cycles of adsorption and regeneration. The CO_2 adsorption was performed at 50 °C, while the regeneration was conducted with the flush of He gas at 200 °C for 30 min. The percentage ratio of the adsorption capacity of the regenerated adsorbent to the virgin one is defined as adsorption index (AI) and is calculated by the formula (3) as follows:

$$\text{AI} = \frac{q_n}{q_1} \times 100\% \quad (3)$$

where, q_n and q_1 denote the CO_2 adsorption capacity of the n^{th} (n = 1–11) cycle and the first cycle, respectively.

3. Results and discussion

3.1 XRD analysis

The crystallinity of the ZIF-8 samples synthesized under different reaction parameters is compared in Fig. 1. The characteristic peaks of ZIF-8 at 2θ value of 7.30°, 10.36°, 12.68°, 16.40° and 17.98° could be clearly observed from the power XRD pattern, indicating the ZIF-8 crystals were formed. As shown in Fig. 1(a), all four zinc salts could form the ZIF-8 crystal in the aqueous solution. Among them, ZIF-8 synthesized with $Zn(NO_3)_2 \cdot 6H_2O$ had the strongest diffraction peak at the (110) plane and thus was used as the reference. The relative crystallinity of ZIF-8 was ranked in the following order: ZIF-8 from $Zn(NO_3)_2 \cdot 6H_2O$ > ZIF-8 from $Zn(OAc)_2 \cdot 2H_2O$ > ZIF-8 from $ZnSO_4 \cdot 7H_2O$ > ZIF-8 from $ZnCl_2$. The influences of the pH value on the relative crystallinity of ZIF-8 are shown in Fig. 1(b). The crystallinity was observed to be the highest when pH = 11.4, and decreased irregularly as the pH value changed. This phenomenon can be attributed that 2-methylimidazole is more likely to be protonated and then more reactive sites are produced on the ligands to facilitate the reaction with Zn^{2+} at the pH of 11.4.[33] Fig. 1(c) showed that the crystallinity was the highest when the reaction temperature was set as 85 °C. According to Fig. 1(d), the relative crystallinity was found to be increased with increased reaction time, and almost kept constant after 360 min due to the completeness of the reaction. The reaction stoichiometry ratio between the zinc resources and 2-methylimidazole (Zn/Hmim) is supposed to be 1 : 2 for the ZIF-8 synthesis. However, Cravillon *et al.* found the addition of excess 2-methylimidazole was necessary in the aqueous solution, and Zn/

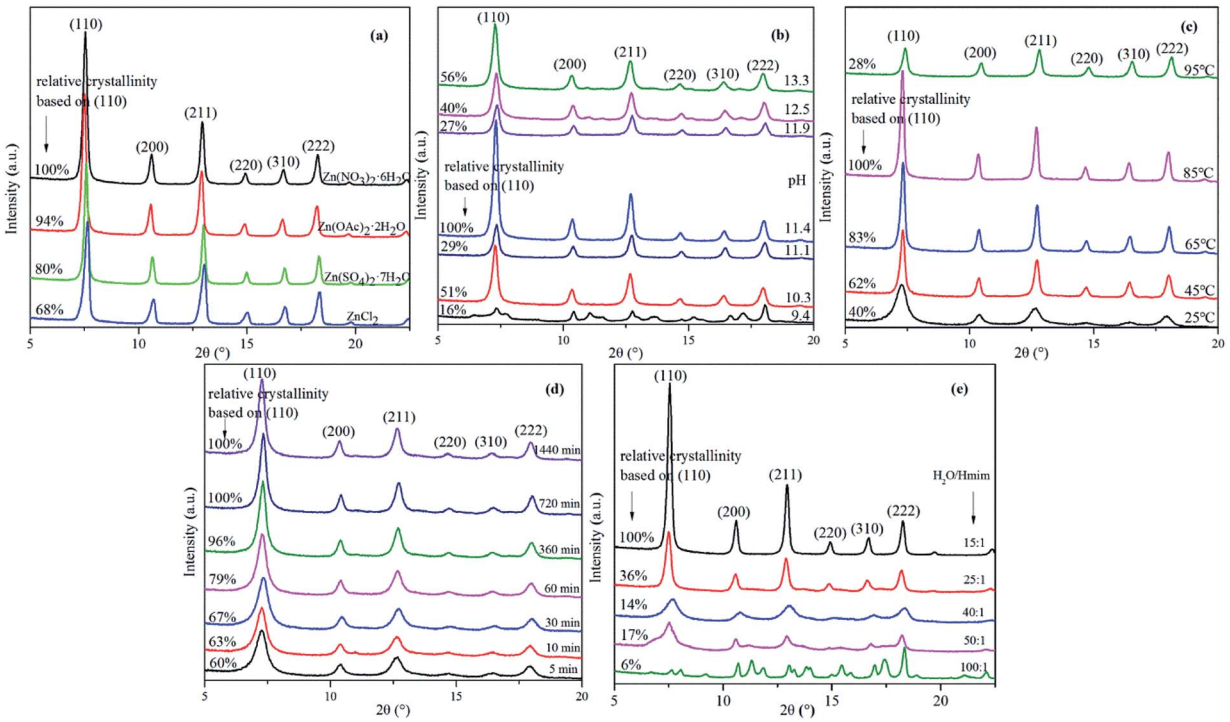

Fig. 1 XRD of ZIF-8 synthesized with different parameters: (a) metal resources: $Zn(NO_3)_2 \cdot 6H_2O$, $Zn(OAc)_2 \cdot 2H_2O$, $ZnSO_4 \cdot 7H_2O$ and $ZnCl_2$; (b) pH value: 9.4, 10.1, 11.1, 11.4, 11.9, 12.5 and 13.3; (c) temperature: 25, 45, 65, 85 and 95 °C; (d) time: 5, 10, 30, 60, 360, 720 and 1440 min; (e) H_2O/Hmim: 15 : 1, 25 : 1, 40 : 1, 50 : 1, 100 : 1.

Hmim was set as 1 : 70 in their study.[23] In order to decrease the amount of 2-methylimidazole, water concentration (H_2O/Hmim) is investigated and the results are shown in Fig. 1(e). It can be seen that the relative crystallinity tended to increase with decreased H_2O/Hmim. The reason is that the deprotonation processes of 2-methylimidazole are difficult because of its high pK_a value in the aqueous solution. Since H_2O/Hmim decreased and the concentration of the 2-methylimidazole became higher, 2-methylimidazole with a high concentration can be regarded as the deprotonation agent due to its alkalinity, then the main crystal surface of ZIF-8 started to form when the reaction ratio is changed to 1 : 20 in this study, and thus save about 70% dosage of 2-methylimidazole in a single reaction.

3.2 N_2 adsorption isotherm

The N_2 adsorption–desorption curves of ZIF-8 synthesized under different reaction parameters are shown in Fig. S1 (ESI†). The Brunauer–Emmett–Teller specific surface area and pore volume are compared as shown in Tables 1–3. The results show that the ZIF-8 samples had larger specific surface areas and pore volumes when higher temperature, longer reaction time and lower water concentration was used in the process of synthesis. As the reaction temperature increased from 25 to 95 °C, the specific surface area firstly increased from 878.59 to 1140.93 m^2 g^{-1}, then decreased to 1017.73 m^2 g^{-1} and the pore volume increased from 0.50 to 0.61 m^3 g^{-1}, which are consistent with the surface areas and pore volumes of the ZIF-8 samples prepared at room temperature.[13,23,42,43] The specific surface area and the pore volume showed the same trends with the increase of the reaction time. It is worth noting that the specific surface area and the pore volume was only 85.56 m^2 g^{-1} and 0.04 m^3 g^{-1} when H_2O/Hmim was 100 : 1, which might be due to the presence of amorphous materials in the ZIF-8 samples.[38] The results are consistent with the relative crystallinity as shown in Fig. 1.

3.3 SEM

The effects of synthesis conditions on the morphology of ZIF-8 samples were evaluated using SEM, and the results are presented in Fig. 2. The effect of temperature is illustrated in Fig. 2(a) and (b), the selected samples were synthesized at 45 °C and 85 °C. The results show that the shape was more structured with fewer surface defects, correlating with the higher relative crystallinity as shown in Fig. 1(b). With the increase of the synthesis time from 5 min to 360 min as shown in Fig. 2(c)–(e),

Table 1 Effect of the reaction temperature on N_2 adsorption

Samples[a]	Temperature (°C)	S_{BET} (m^2 g^{-1})	V_t (cm^3 g^{-1})
A3	25	878.59	0.50
B3	45	1019.62	0.54
C3	65	1140.93	0.59
D3	85	1146.35	0.60
E3	95	1017.73	0.61

[a] The denotation and the corresponding synthesized parameters of all the samples can be found in the ESI.

Table 2 Effect of the reaction time on N_2 adsorption

Samples[a]	Time (min)	S_{BET} (m^2 g^{-1})	V_t (cm^3 g^{-1})
A4	5	878.59	0.50
C4	30	899.28	0.52
D4	60	923.01	0.54
E4	360	937.06	0.55
G4	1440	1027.20	0.59

[a] The denotation and the corresponding synthesized parameters of all the samples can be found in the ESI.

Table 3 Effect of the water concentration on N_2 adsorption

Samples[a]	H_2O/Hmim	S_{BET} (m^2 g^{-1})	V_t (cm^3 g^{-1})
A5	15 : 1	1210.11	0.65
B5	25 : 1	841.72	0.46
C5	40 : 1	645.57	0.36
D5	50 : 1	603.53	0.32
E5	100 : 1	85.56	0.04

[a] The denotation and the corresponding synthesized parameters of all the samples can be found in the ESI.

a rugged surface was obtained first, and then rod-like particles started to form. The growth of the crystal over time could be observed, but it is worth noting that the shape was unusual, though their XRD patterns exhibited a typical ZIF-8 crystallinity phase. The influence of water concentration is presented in Fig. 2(f)–(h), which show the ZIF-8 crystal prepared with H_2O/Hmim as 15 : 1 was spherical and had a bumpy surface. The morphology was changed to a small dense cylinder first, and then to a lager cylinder with low crystallinity as H_2O/Hmim increased to 40 : 1 and 100 : 1, respectively. This is because when H_2O/Hmim increased, the pH of the solution decreased.

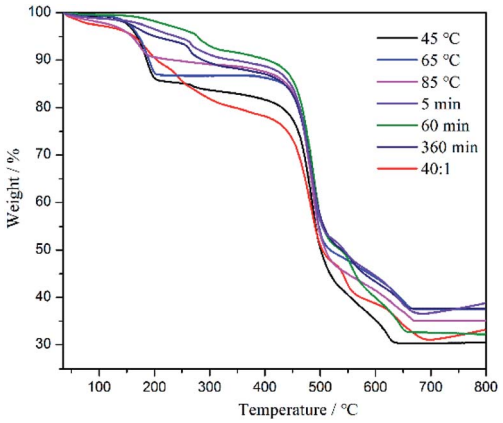

Fig. 3 TGA of ZIF-8 synthesized under different synthesis conditions: 45 °C, 65 °C, 85 °C, 5 min, 60 min, 360 min, and H_2O/Hmim = 40 : 1.

Under the decreased pH, 2-methylimidazole was deprotonated slowly, which in turn postponed the formation of the ZIF-8 crystals.[43]

3.4 TGA analysis

The thermogravimetric analysis experiments were conducted under air flow to characterize the thermal stability of the ZIF-8 samples. As shown in Fig. 3, the first mass loss below 250 °C might be caused by the removal of guest molecules (*e.g.* H_2O) from the cavities or residual species (2-methylimidazole), which is comparable to that in the literature.[30] Between 250 °C and 445 °C, a long plateau was observed after the formation of the guest-free phase, indicating a good thermal stability of the ZIF-8 samples. The second mass loss around 445 °C indicates that the structure of the sample began to collapse. By comparison, the thermal stability did not change with the varying synthesis conditions, so long as the ZIF-8 crystal was completely formed.

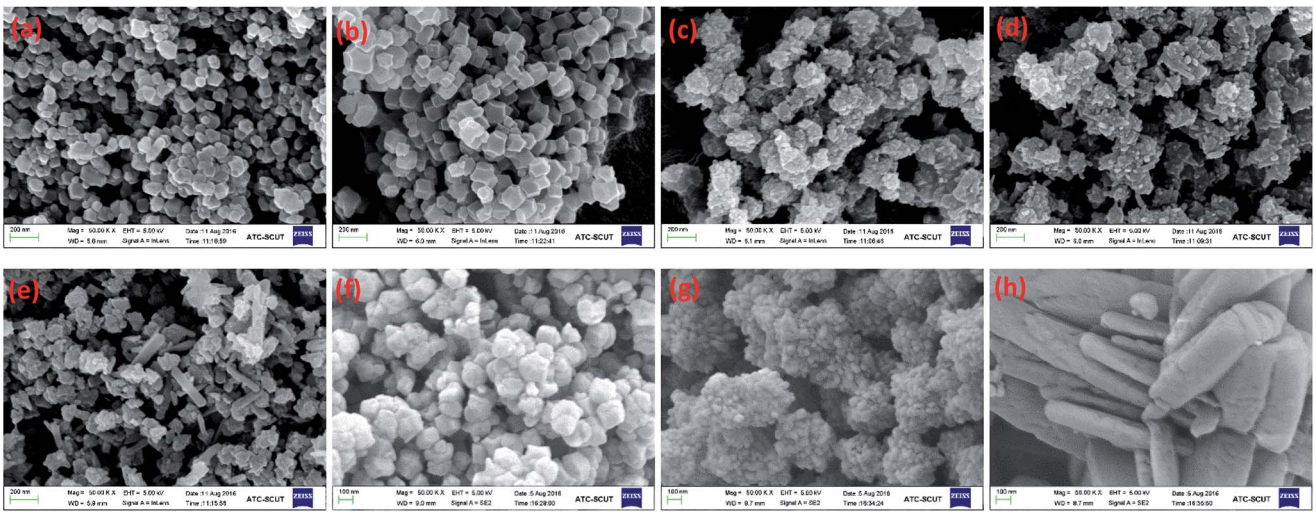

Fig. 2 SEM images of ZIF-8 synthesized under different conditions: (a and b) T = 45 °C, 85 °C; (c–e) t = 5 min, 60 min, and 360 min; (f–h) H_2O/Hmim = 15 : 1, 40 : 1, and 100 : 1.

Table 4 Effects of the synthesis temperature on CO_2 adsorption capacity

		CO_2 adsorption capacity q/mmol g^{-1}				
Samples	Temperature (°C)	35 °C	45 °C	55 °C	65 °C	75 °C
B3	45	2.57	2.42	2.29	2.18	2.18
C3	65	2.96	2.86	2.67	2.65	2.57
D3	85	3.04	2.90	2.82	2.70	2.51
E3	95	2.60	2.53	2.46	2.41	2.32

Table 5 Effects of the reaction time on CO_2 adsorption capacity

		CO_2 adsorption capacity q/mmol g^{-1}				
Samples	Time (min)	35 °C	45 °C	55 °C	65 °C	75 °C
A4	5	2.60	2.52	2.45	2.38	2.24
C4	30	2.78	2.72	2.59	2.53	2.40
D4	60	2.82	2.72	2.62	2.61	2.55
E4	360	2.87	2.79	2.62	2.54	2.49
G4	1440	2.94	2.78	2.70	2.65	2.49

Table 6 Effects of the water concentration on CO_2 adsorption capacity

		CO_2 adsorption capacity q/mmol g^{-1}				
Sample	H_2O/Hmim	35 °C	45 °C	55 °C	65 °C	75 °C
A5	15 : 1	2.78	2.67	2.53	2.46	2.35
C5	40 : 1	2.64	2.55	2.46	2.39	2.29
D5	50 : 1	2.60	2.48	2.40	2.27	2.26

3.5 CO_2 adsorption

The CO_2 adsorption with the ZIF-8 samples was studied as described in the Experimental section. The breakthrough curves of the ZIF-8 samples are shown in Fig. S3–S5.† And the CO_2 adsorption capacities of the corresponding samples at the different adsorption temperature can be found in Tables 4–6. From Fig. S3–S5† and Tables 4–6, it can be seen that under the same synthesis condition, the CO_2 adsorption capacity of ZIF-8 decreased continually when the adsorption temperature increased from 35 °C to 75 °C. This phenomenon can be attributed to the fact that the increase of the temperature leads to the decrease of van der Waals' force between CO_2 molecules and the samples. At the same adsorption temperature, the CO_2 adsorption capacity of ZIF-8 varied as the synthesis condition changed. It can be seen from Table 4 that as the synthesis temperature increased from 45 °C to 95 °C, the CO_2 adsorption capacity of ZIF-8 at 35 °C firstly increased from 2.57 mmol g^{-1} to 3.04 mmol g^{-1}, then decreased to 2.60 mmol g^{-1}. This trend is consistent with the BET specific surface area. Table 5 shows the effect of the synthesis time of ZIF-8 on the CO_2 adsorption capacity. The results show the ZIF-8 sample had the highest CO_2 adsorption capacity (2.94 mmol g^{-1}) when synthesized under 1440 min. In Table 6, it shows that the CO_2 adsorption capacity of ZIF-8 decreased when H_2O/Hmim increased, and similarly, the changes of the water concentration had the same effect on the BET specific surface area and pore volume. These results further demonstrate that the CO_2 adsorption capacity of ZIF-8 is closely related to its BET specific surface area and pore volume.

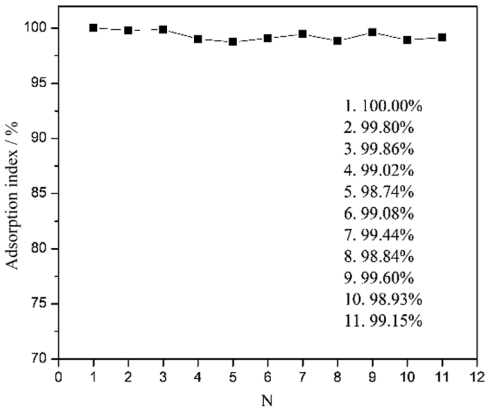

Fig. 4 CO_2 cyclic adsorption performance of ZIF-8 synthesized in the aqueous solution.

The prolonged cyclic CO_2 adsorption on ZIF-8 was conducted as mentioned in the Experimental section, and the results are shown in Fig. 4. The results show that the adsorption index was only reduced from 100% to 99.15% at the 11th run, suggesting that most CO_2 molecules can be effectively desorbed during the regeneration process, and the ZIF-8 samples in the present study are satisfactorily stable and effective in the prolonged cyclic operation.

4. Conclusions

In summary, we have synthesized ZIF-8 in aqueous solutions, and the influences of key operating parameters are investigated. The XRD analysis shows that the ZIF-8 crystal produced from $Zn(NO_3)_2 \cdot 6H_2O$ exhibited the highest crystallinity. The pH value had a big impact because it influences the protonation states of 2-methylimidazole. High temperature, long reaction time, and low water concentration are also found to be favourable in the formation of high crystallinity. The BET results show that surface area and pore volume increased gradually with the increase of temperature and reaction time, and the decrease of water concentration. The CO_2 adsorption results show that the physical adsorption of ZIF-8 on CO_2 dominated the adsorptive mode. And the experimental results imply that the CO_2 adsorption capacity is influenced primarily by the BET specific surface area and pore volume rather than the relative crystallinity. Meanwhile, the high CO_2 adsorption capacity and excellent cycling performance of these samples indicate that the water-based synthesis of ZIF-8 is a promising way for CO_2 capture.

Acknowledgements

This research was supported by the financial support of the National Natural Science Foundation of China (Grant No.

21006035, 21176088 and 21676099), and the Doctoral Fund of Ministry of Education of China.

Notes and references

1 A. Hussain, *Sep. Sci. Technol.*, 2012, **47**, 1857–1865.
2 T. Schneider, J. Teixeira, C. S. Bretherton, F. Brient, K. G. Pressel, C. Schär and A. P. Siebesma, *Nat. Clim. Change*, 2017, **7**, 3–5.
3 T. M. Lenton, *Clim. Change*, 2006, **76**, 7–29.
4 R. Sakwattanapong, A. Aroonwilas and A. Veawab, *Ind. Eng. Chem. Res.*, 2005, **44**, 4465–4473.
5 L. F. Ding and A. O. Yazaydin, *Phys. Chem. Chem. Phys.*, 2013, **15**, 11856–11861.
6 A. Chakma and A. Meisen, *Ind. Eng. Chem. Prod. Res. Dev.*, 1986, **25**, 627–630.
7 Y. D. Tang and K. Landskron, *J. Phys. Chem. C*, 2010, **114**, 2494–2498.
8 Q. Wang, J. Z. Luo, Z. Y. Zhong and A. Borgna, *Energy Environ. Sci.*, 2011, **4**, 42–55.
9 S. D. Kenarsari, D. L. Yang, G. D. Jiang, S. J. Zhang, J. J. Wang, A. G. Russell, Q. Wei and M. H. Fan, *RSC Adv.*, 2013, **3**, 22739–22773.
10 J. Y. Wang, L. Huang, R. Y. Yang, Z. Zhang, J. W. Wu, Y. S. Gao, Q. Wang, D. O'Hare and Z. Y. Zhong, *Energy Environ. Sci.*, 2014, **7**, 3478–3518.
11 B. Sreenivasulu and I. Sreedhar, *Environ. Sci. Technol.*, 2015, **49**, 12641–12661.
12 R. Banerjee, A. Phan, B. Wang, C. Knobler, H. Furukawa, M. O'Keeffe and O. M. Yaghi, *Science*, 2008, **319**, 939–943.
13 K. S. Park, Z. Ni, A. P. Côté, J. Y. Choi, R. Huang, F. J. Uribe-Romo, H. K. Chae, M. O'Keeffe and O. M. Yaghi, *Proc. Natl. Acad. Sci. U. S. A.*, 2006, **103**, 10186–10191.
14 Y. Hu, Z. Liu, J. Xu, Y. N. Huang and Y. Song, *J. Am. Chem. Soc.*, 2013, **135**, 9287–9290.
15 L. L. Zhang, G. Wu and J. W. Jiang, *J. Phys. Chem. C*, 2014, **118**, 8788–8794.
16 S. Gadipelli, W. Travis, W. Zhou and Z. X. Guo, *Energy Environ. Sci.*, 2014, **7**, 2232–2238.
17 Z. J. Zhang, S. K. Xian, Q. B. Xia, H. H. Wang, Z. Li and J. Li, *AIChE J.*, 2013, **59**, 2195–2206.
18 R. Kumar, K. Jayaramulu, T. K. Maji and C. N. R. Rao, *Chem. Commun.*, 2013, **49**, 4947–4949.
19 R. Li, X. Q. Ren, X. Feng, X. G. Li, C. W. Hu and B. Wang, *Chem. Commun.*, 2014, **50**, 6894–6897.
20 T. Chokbunpiam, S. Fritzsche, C. Chmelik, J. Caro, W. Janke and S. Hannongbua, *Chem. Phys. Lett.*, 2016, **648**, 178–181.
21 P. Puphasuk and T. Remsungnen, *Chem. Phys. Lett.*, 2016, **647**, 20–25.
22 X. C. Ma, L. Q. Li, S. B. Wang, M. M. Lu, H. L. Li, W. W. Ma and T. C. Keener, *Appl. Surf. Sci.*, 2016, **369**, 390–397.
23 J. Cravillon, S. Munzer, S. J. Lohmeier, A. Feldhoff, K. Huber and M. Wiebcke, *Chem. Mater.*, 2009, **21**, 1410–1412.
24 X. L. Liu, Y. S. Li, Y. J. Ban, Y. Peng and H. Jin, *Mater. Lett.*, 2014, **136**, 341–344.
25 B. Seoane, J. M. Zamaro, C. Tellez and J. Coroas, *RSC Adv.*, 2011, **1**, 917–922.
26 H. Bux, F. Y. Liang, Y. S. Li, J. Cravillon, M. Wiebcke and J. CaroZeolitic, *J. Am. Chem. Soc.*, 2009, **131**, 16000–16001.
27 M. J. Cliffe, C. Mottillo, R. S. Stein, D. K. Bucar and T. Friscic, *Chem. Sci.*, 2012, **3**, 2495–2500.
28 T. T. Xing, Y. B. Lou, Q. L. Bao and J. X. Chen, *CrystEngComm*, 2014, **16**, 8994–9000.
29 B. Seoane, J. M. Zamaro, C. Tellez and J. Coronas, *CrystEngComm*, 2012, **14**, 3103–3107.
30 X. J. Zhao, X. L. Fang, B. H. Wu, L. S. Zheng and N. F. Zheng, *Sci. China: Chem.*, 2014, **57**, 141–146.
31 Y. C. Pan, Y. Y. Liu, G. F. Zeng, L. Zhao and Z. P. Lai, *Chem. Commun.*, 2011, **47**, 2071–2073.
32 J. F. Yao, M. He, K. Wang, R. Z. Chen, Z. X. Zhong and H. T. Wang, *CrystEngComm*, 2013, **15**, 3601–3606.
33 N. A. H. M. Nordin, A. F. Ismail, A. Mustafa, P. S. Goh, D. Rana and T. Matuura, *RSC Adv.*, 2014, **4**, 33292–33300.
34 B. L. Chen, F. H. Bai, Y. Q. Zhu and Y. D. Xia, *Microporous Mesoporous Mater.*, 2014, **193**, 7–14.
35 Q. Wang, J. F. Bai and Z. Y. Lu, *Chem. Commun.*, 2016, **52**, 443–452.
36 F. K. Shieh, S. C. Wang, S. Y. Leo and K. C.-W. Wu, *Chem.–Eur. J.*, 2013, **19**, 11139–11142.
37 Y. X. Sun and W. Y. Sun, *Chin. Chem. Lett.*, 2014, **25**, 823–828.
38 L. S. Lai, Y. F. Yeong, N. C. Ani, K. K. Lau and A. M. Shariff, *Part. Sci. Technol.*, 2014, **32**, 520–528.
39 K. Kida, M. Okita, K. Fujita, S. Tanaka and Y. Miyake, *CrystEngComm*, 2013, **15**, 1794–1801.
40 E. L. Bustamante, J. L. Fernandez and J. M. Zamaro, *J. Colloid Interface Sci.*, 2014, **424**, 37–43.
41 C. Wei Tsai and E. H. G. Langner, *Microporous Mesoporous Mater.*, 2016, **221**, 8–13.
42 S. K. Nune, P. K. Thallapally, A. Dohnalkova, C. M. Wang, J. Liu and G. J. Exarhos, *Chem. Commun.*, 2010, **46**, 4878–4880.
43 M. P. Jian, B. Liu, R. P. Liu, J. H. Qu, H. T. Wang and X. W. Zhang, *RSC Adv.*, 2015, **5**, 48433–48441.